Landau level spectrum and magneto-optical conductivity in tilted Weyl semimetal

Pu Liu,[1,2] Chaoxi Cui,[1,2] Xiao-Ping Li,[3,*] Zhi-Ming Yu,[1,2,†] and Yugui Yao[1,2]

[1]*Centre for Quantum Physics, Key Laboratory of Advanced Optoelectronic Quantum Architecture and Measurement (MOE), School of Physics, Beijing Institute of Technology, Beijing 100081, China*

[2]*Beijing Key Lab of Nanophotonics & Ultrafine Optoelectronic Systems, School of Physics, Beijing Institute of Technology, Beijing 100081, China*

[3]*School of Physical Science and Technology, Inner Mongolia University, Hohhot 010021, China*

(Received 7 December 2022; accepted 17 February 2023; published 27 February 2023)

We present a systematic investigation of the magnetoresponses of the Weyl points (WPs) with a topological charge of $n = 2,\ 3$, and 4, and with both linear and quadratic energy tilt. The linear tilt always tends to squeeze the Landau levels (LLs) of both conduction and valence bands of all the WPs, and eventually leads to LL collapse in the type-II phase. However, the quadratic energy tilt has more complex influences on the LLs of the unconventional WPs. For charge-n ($n = 2, 4$) WP, the influence of the quadratic tilt on the LLs of conduction and valence bands are opposite, i.e., if the LLs of conduction (valence) bands are squeezed, then that of the valence (conduction) bands are broadened and the squeezed LL spectrum will be collapsed in the type-III phase. But, the LL collapse generally cannot be found in the type-III charge-3 WP. Moreover, for charge-n ($n = 2, 3$) WP, the quadratic tilt breaks the degeneracy of the chiral LLs regardless of the direction of the magnetic field, leading to additional optical transitions and magneto-optical conductivity peaks at low frequencies. Interestingly, the four chiral LLs in charge-4 WP are always not degenerate. Hence there inevitably exist magneto-optical conductivity peaks at low frequencies for charge-4 WP. Since the density of state of the LL spectrum is very large, one can expect that the low-frequency magneto-optical responses in unconventional WPs would be significant and may be used for developing efficient terahertz photodetectors.

DOI: 10.1103/PhysRevB.107.085146

I. INTRODUCTION

Weyl semimetal, a novel topological state of matter that possess momentum-space singularities, has been attracting broad interests in current research [1,2]. Such singularity, named as Weyl point (WP), is a kind of double degeneracy formed by nondegenerate conduction and valence bands [3]. Around the degeneracy, the conventional WP exhibits linear dispersion along any direction in momentum space, respecting the Weyl equation proposed in high-energy physics [3]. Henceeach conventional WP is assigned a chirality (unit topological charge) with $|\mathcal{C}| = 1$.

However, the crystals do not have Lorentz symmetry and hence the WP in crystals can take different forms, generally manifested in two aspects. The first one is that, with certain symmetries such as rotation axis, multiple conventional Weyl points with the same topological charge can merge together, leading to unconventional WPs [4–6]. Recently, we show that there are only three possibilities for the crystalline-symmetry protected unconventional WPs [6–8], which have topological charge $|\mathcal{C}| = 2,\ 3$, and 4, respectively. The charge-2 (C-2) and C-3 WPs exhibit linear dispersion along rotation axis and nonlinear dispersion in the plane normal to rotation axis [5]. More interestingly, the C-4 WP features nonlinear dispersion along any direction in momentum space [6,9,10]. The second aspect is the tilt of the Weyl cone, as many energy tilt terms are compatible with the crystalline symmetry. For conventional C-1 WP, only the linear energy term is relevant, as the leading order of $\boldsymbol{k}$ in the corresponding Hamiltonian is linear. But for C-2 and C-3 WPs, both linear and quadratic energy tilt terms are relevant and symmetry allowed [5,6]. Because the C-4 WP is located at the high-symmetry point with time-reversal symmetry $\mathcal{T}$ or $\mathcal{T}' = \mathcal{T}|t_0$ with t_0 a half lattice translation [6–8], which forbids the linear energy tilt, hence it has only quadratic energy tilt.

Both linear and quadratic energy tilt do not change the essential topological properties of the WPs, such as topological charge, but they do have important influence on the geometry of the Fermi surface. By increasing the linear energy tilt, the C-n ($n = 1, 2, 3$) WP will undergo a phase transition from type-I WP to type-II WP [11], for which the Fermi surfaces respectively are a point and a surface constructed by electron pocket and hole pocket. Similarly, the quadratic energy tilt also can transform the Fermi surface of C-n ($n = 2, 3, 4$) WP from a point to a surface, but which here is constructed by two electron or hole pockets [12], distinct from the case in type-II WP. Such WPs hence are referred to as type III to be distinguished from the type-II ones. Since most of the material properties are determined by the geometry of Fermi surface and the density of states around Fermi level, one can expect that the WPs with different topological charge or with and without energy tilt will exhibit completely different

*xpli@imu.edu.cn
†zhiming_yu@bit.edu.cn

signatures, which is also an important basis for experimentally identifying these topological states [13–18]. Many materials have recently been predicted as the unconventional Weyl semimetals [9,12,19–22]. Particularly, nonmagnetic material $(TaSe_4)_2I$ and magnetic materials X_2RhF_6 and $BaNiIO_6$ are predicted as type-III Weyl semimetals [12,19,20]. The C-4 WP has been reported in the electronic band structure of BaIrP without spin-orbit coupling [9].

Magneto-optical conductivity can serve as an experimental tool for observing salient features of systems, which are not available in direct-current measurement [23–25]. For example, the information like energy gap and Fermi velocity of the band structure of systems can be extracted from these resonant peaks of the optical conductivity [26–32]. Hence optical spectrum measurement is a standard and fundamental approach to detect and understand the band structure of target materials. Recently, the magneto-optical conductivity of topological Weyl semimetals has been studied by several works [33–36]. Ashby and Carbotte studied the magneto-optical conductivity of the C-1 WP without energy tilt for different Fermi levels and scattering rates [33]. By introducing linear energy tilt, the C-1 WP becomes anisotropic and the LLs of the system would have a strong dependence on the direction of the B field [37]. Particularly, in the type-II phase, the LLs of C-1 WP would be collapsed at a critical angle between the B field and the tilt, and the magneto-optical conductivity is distinguished from that of type-I C-1 WP [37–39]. The magneto-optical conductivity of C-2 and C-3 WPs with and without linear energy tilt were also investigated in Refs. [39–42]. However, the magnetoresponse of recently proposed C-4 WP and that of the C-n ($n = 2, 3$) WPs with quadratic energy tilt has yet not been explored.

In this work, we present a systematic investigation of the magnetoresponse of unconventional WPs with both linear and quadratic energy tilt, based on the low-energy effective Hamiltonian and Kubo formula. We find that, for C-2 and C-4 WPs, the additional quadratic energy tilt tends to squeeze the LLs of one of the valence and conduction bands and broadens the LLs of the other band. Hence, when quadratic energy tilt is large and the C-2 (C-4) WP becomes the type-III one, only valence or conduction band features LL collapse, which is in sharp contrast to the type-II WPs, where the LLs of both valence and conduction bands collapse [37]. Interestingly, the LL collapse generally cannot be realized in C-3 WP regardless of the presence or absence of the quadratic energy tilt.

The quadratic energy tilt also has important influence on the magneto-optical conductivity of the unconventional WPs. In the absence of quadratic energy tilt, both C-2 and C-3 WPs have degenerate chiral LLs when the B field is parallel to the principal rotation axis of systems [36,43]. Such degeneracy will be broken by the quadratic energy tilt, which makes a new transition between the chiral LLs and leads to additional peak(s) in the magneto-optical conductivity spectrum at low frequencies. At the same time, the original longitudinal magneto-optical conductivity peaks will be split and the original transverse magneto-optical conductivity changes from zero to a series of positive and negative peaks. But, the four chiral LLs in C-4 Weyl point are always not degenerate [6,44] and the absorption peaks from the transition between different chiral LLs generally are much more significant than that in C-2 and C-3 WPs. Besides, similar to the previous investigation on type-II WPs [37], the type-III WPs exhibit many intraband absorption peaks at low frequencies.

This paper is organized as follows. In Sec. II, we analytically calculate the LLs for C-2 and C-3 WPs with both linear and quadratic energy tilt when the magnetic field is along the z direction and numerically calculate the LL spectrum of C-n ($n = 2, 3, 4$) WPs with different tilt parameters. Beside, we discuss the LL collapse in the unconventional WPs based on a semiclassical picture. Then, in Sec. III, we present the magneto-optical transition selection rules and show the numerical results for the corresponding magneto-optical conductivity for C-n ($n = 2, 3, 4$). At last, we summarize our results in Sec. IV.

II. LL SPECTRUM

A. C-2 and C-3 WPs

A general low-energy effective Hamiltonian of C-2 (C-3) WP without energy tilt can be written as [6]

$$\mathcal{H}_0 = v_z k_z \sigma_z + \lambda(k_-^m \sigma_+ + k_+^m \sigma_-), \tag{1}$$

where v_z and λ are real model parameters, $m = 2$ ($m = 3$), $\sigma_\pm = (\sigma_x \pm i\sigma_y)/2$ with σ_i ($i = x, y, z$) the Pauli matrix, and $k_\pm = k_x \pm ik_y$. One observes that the leading order of $\boldsymbol{k}$ in the effective Hamiltonian (1) along the k_z direction is linear and that in k_x-k_y plane is quadratic (cubic) for $m = 2$ ($m = 3$). Hence a linear energy tilt term $\propto k_i$ will compete with $v_z k_z \sigma_z$ along the k_z direction and dominate the energy dispersion around the WP in the k_x-k_y plane. In practice, however, the C-2 and C-3 WPs are located at high-symmetry line (k_z axis here) with multiple-fold rotation symmetry, which forbids the appearance of linear and cubic terms in the k_x-k_y plane [6]. Consequently, the relevant energy tilt for C-2 (C-3) WP includes two parts: A linear energy tilt along the k_z direction and a quadratic energy tilt in the k_x-k_y plane, for which the effective Hamiltonians read

$$\mathcal{H}_{tilt} = w_z k_z + w_{||} k_{||}^2, \tag{2}$$

with $k_\parallel = \sqrt{k_x^2 + k_y^2}$. The energy dispersion of the C-m ($m = 2, 3$) WP with energy tilt (2) is

$$E_\pm = w_z k_z + w_{||} k_{||}^2 \pm \sqrt{v_z^2 k_z^2 + \lambda^2 k_\parallel^{2m}}. \tag{3}$$

When $|w_z| > |v_z|$, the Weyl cone is overtilted, leading to a type-II C-2 (C-3) WP. But the influence of quadratic energy tilt on C-2 and C-3 WP is different, which then leads to different consequences for the LL spectrum, as shown below. For C-2 WP, it becomes a type-III WP when $|w_{||}| > |\lambda|$, as its band structure in the k_x-k_y plane is $E_\pm = (w_{||} \pm \lambda)k_{||}^2$. For C-3 WP with energy tilt, its energy dispersion in the k_x-k_y plane is $E_\pm = w_{||} k_{||}^2 \pm \lambda k_\parallel^3$, indicating the band structure of C-3 WP is dominated by $w_{||} k_{||}^2$ for small $k_\parallel$. Hence an arbitrary small $|\lambda|$ can transform a type-I C-3 WP to a type-III one. But, it should be noticed that, for large $k_\parallel$, the band structure of C-3 WP is dominated by $\pm\lambda k_\parallel^3$.

We first consider a uniform magnetic field along the z direction, as in such case the LL spectrum of C-2 (C-3) WP can be analytically obtained. Notice that, in the following calculations, we have neglected the Zeeman effect induced by

magnetic field, as it is much smaller than the orbital effect at accessible field strength. We make the usual Peierls substitution $\boldsymbol{k} \to \boldsymbol{\Pi} = \boldsymbol{k} + e\boldsymbol{A}/\hbar$ in the effective Hamiltonian with the vector potential $\boldsymbol{A} = (0, Bx, 0)$. Here, we have chosen the Landau gauge. By introducing the creation and annihilation operators

$$\hat{a} = \frac{l_B}{\sqrt{2}\hbar}(\Pi_x - i\Pi_y), \quad \hat{a}^\dagger = \frac{l_B}{\sqrt{2}\hbar}(\Pi_x + i\Pi_y), \tag{4}$$

the Hamiltonian $\mathcal{H} = \mathcal{H}_0 + \mathcal{H}_{tilt}$ can be rewritten as

$$H = w_z k_z + v_z k_z \sigma_z + \omega_{||}(2\hat{a}^\dagger \hat{a} + 1) + \lambda\left(\frac{\sqrt{2}}{l_B}\right)^m [\hat{a}^m \sigma_+ + (\hat{a}^\dagger)^m \sigma_-], \tag{5}$$

where $l_B = \sqrt{\hbar/eB}$ denotes the magnetic length and $\omega_{||} = w_{||}/l_B^2$.

After straightforward calculations, the LL spectrum and the eigenstates of C-2 WP ($m = 2$) are obtained as

$$\varepsilon_n(k_z) = (2|n| + 1)\omega_{||} + (w_z - v_z)k_z, \tag{6}$$

$$\Psi_n = (0, |n\rangle)^T, \tag{7}$$

for $n = 0, 1$, and

$$\varepsilon_n(k_z) = (2|n| - 1)\omega_{||} + w_z k_z + \mathrm{sgn}(n)\Gamma_n(k_z), \tag{8}$$

$$\Psi_n = (\alpha_n||n| - 2\rangle, \beta_n||n|\rangle)^T, \tag{9}$$

for $|n| \geqslant 2$ with

$$\Gamma_n(k_z) = \sqrt{(v_z k_z - 2\omega_{||})^2 + \frac{4\lambda^2}{l_B^4}|n|(|n| - 1)}, \tag{10}$$

$$\alpha_n = \sqrt{\frac{\mathrm{sgn}(n) \times (v_z k_z - 2\omega_{||}) + \Gamma(k_z)}{2\Gamma(k_z)}}, \tag{11}$$

$$\beta_n = \sqrt{\frac{-\mathrm{sgn}(n) \times (v_z k_z - 2\omega_{||}) + \Gamma(k_z)}{2\Gamma(k_z)}}, \tag{12}$$

and $|n\rangle$ the harmonic oscillator eigenstate.

Similarly, the LL spectrum and the eigenstates of C-3 WP ($m = 3$) are obtained as

$$\varepsilon_n(k_z) = (2|n| + 1)\omega_{||} + (w_z - v_z)k_z, \tag{13}$$

$$\Psi_n = (0, |n\rangle)^T, \tag{14}$$

for $n = 0, 1, 2$, and

$$\varepsilon_n(k_z) = 2(|n| - 1)\omega_{||} + w_z k_z + \mathrm{sgn}(n)\Gamma'_n(k_z), \tag{15}$$

$$\Psi_n = (\alpha'_n||n| - 3\rangle, \beta'_n||n|\rangle)^T, \tag{16}$$

for $|n| \geqslant 3$ with

$$\Gamma'_n(k_z) = \sqrt{(v_z k_z - 3\omega_{||})^2 + \frac{8\lambda^2}{l_B^6}|n|(|n| - 1)(|n| - 2)}, \tag{17}$$

$$\alpha'_n = \sqrt{\frac{\mathrm{sgn}(n) \times (v_z k_z - 3\omega_{||}) + \Gamma'(k_z)}{2\Gamma'(k_z)}}, \tag{18}$$

$$\beta'_n = \sqrt{\frac{-\mathrm{sgn}(n) \times (v_z k_z - 3\omega_{||}) + \Gamma'(k_z)}{2\Gamma'(k_z)}}. \tag{19}$$

The calculated LLs of C-2 and C-3 WPs with different parameters are shown in Fig. 1 and Fig. 2. From Eqs. (8) and (15), one observes that, in the $k_z = 0$ plane, the LL energy of C-2 WP is proportional to the magnetic field B whether there is a tilt term or not, but that of C-3 WP is proportional to $B^{3/2}$ when $w_\parallel = 0$, which is different from the C-1 WP [40]. Besides, we find that the influence of linear and quadratic energy tilt on LLs are completely different. First, as shown in Figs. 1(a)–1(d) and 2(a)–2(d), without any tilt or with only linear tilt, there are two (three) degenerated chiral LLs for C-2 (C-3) WP, consistent with previous results [36,42,43]. But when the quadratic energy tilt is added, the degeneracy of the two (three) chiral bands is broken, as shown in Figs. 1(f)–1(h) [Figs. 2(f)–2(h)]. And, one observes that the splitting of the chiral LLs is more significant for C-2 WP. Moreover, we find that the quadratic energy tilt $[(2|n| \pm 1)w_{||}/l_B^2]$ always tends to elevate the LL bands. Particularly, for type-III C-2 WP ($|w_{||}| > |\lambda|$), all the LLs at the $k_z = 0$ point have positive energy [see Fig. 1(h)]. But, this is not the case for type-III C-3 WP, due to the presence of $k^3_{+(-)}$ terms in the Hamiltonian [Eq. (1)]. Second, the linear energy tilt tends to tilt and squeeze the LL spectrum of C-2 (C-3) WP, while no obvious tilt of the LLs can be observed for the C-2 (C-3) WP with only quadratic energy. Increasing w_z (with $w_\parallel = 0$), the LLs gets more and more tilted and the chiral LLs become flat bands when $w_z = v_z$, as the slope of the chiral LLs is determined by $w_z - v_z$ [see Eqs. (6) and (13)]. When $|w_z| > |v_z|$, the system becomes type-II WPs and the resulting LLs are overtilted. In contrast, increasing $w_{||}$ ($w_{||} > 0$ with $w_z = 0$), the LLs of the valence band will be squeezed, while that of the conduction band are broadened [see Figs. 1(f)–1(h) and Figs. 2(f)–2(h)]. Particularly, for C-2 WP, the valence band at the $k_z = 0$ plane becomes a flat band when $w_{||} = \lambda$. Generally, the LLs of a trivial flat band are all degenerate at the same energy. But, for a nontrival band with finite orbital momentum, its structure will be modified when a magnetic field is applied [37,45–47]. Since the C-2 WP exhibit significant Berry curvature and orbital momentum, the original flat band here is modified to have an energy variation, leading to nondegenerate LLs at $k_z = 0$ plane, as shown in Fig. 1(g). Interestingly, Rhim *et al.* show that, in such case, the LL spacing is determined by the quantum distance of the Bloch states of the Weyl point without external magnetic field [48]. When $|w_\parallel| > |\lambda|$ in C-2 WP and $|w_\parallel| > 0$ in C-3 WP, the systems become type-III WPs and the Fermi surface is no longer a point but contains two hole pockets; then the Fermi level may or may not go through many LLs depending on the size of the two hole pockets and the strength of the B field [see Figs. 1(h) and 2(h)]. When both linear and quadratic energy tilt are added, not only does the band tilt, but also the degeneracy of the chiral LLs is broken, as shown in Figs. 1(e) and 2(e).

When the B field deviates from the z direction, it is generally difficult to obtain analytical expressions for the LL spectrum. Alternatively, we calculate it numerically. It was shown that the type-II C-1 WP features LL collapse, which can be quantitatively understood within a semiclassical

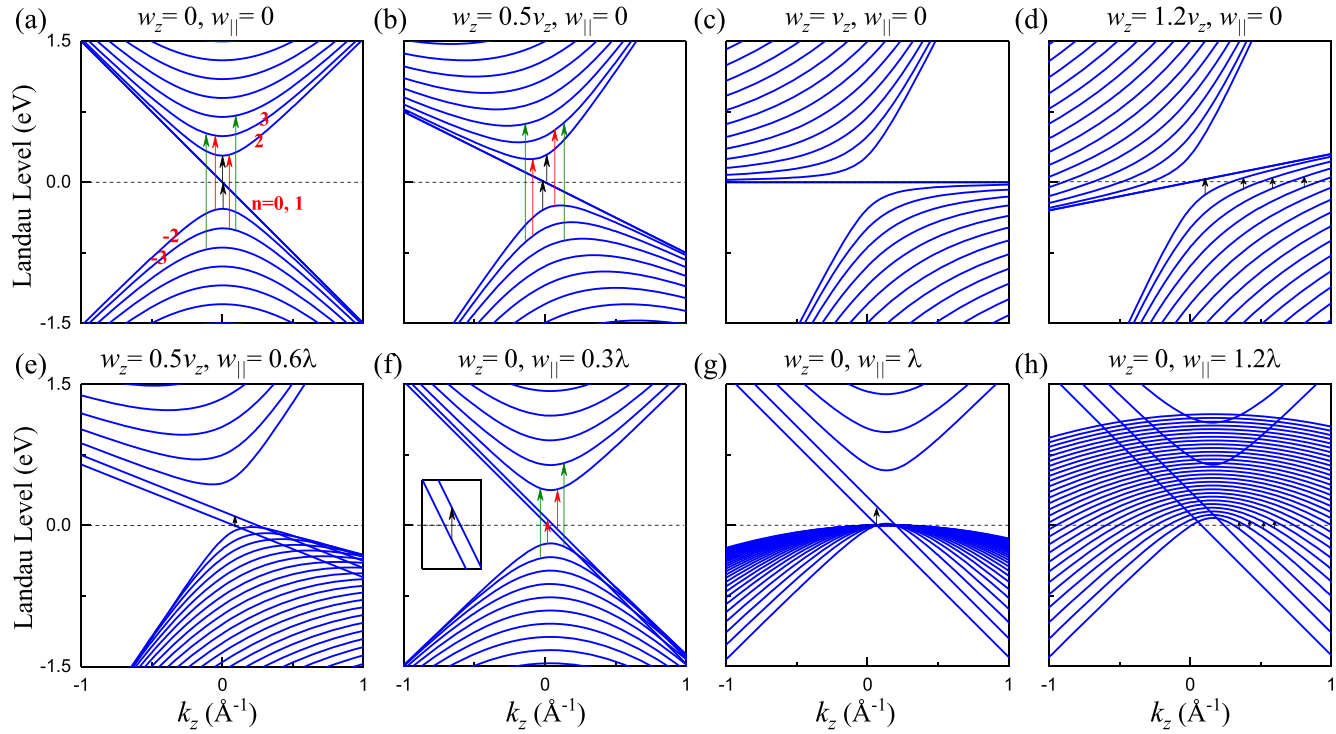

FIG. 1. LL spectrum of the C-2 WPs along k_z with different energy tilts. We set $v_z = 1.5$ eV Å, $\lambda = 0.1$ eV Å^2, and $l_B = 1$ Å. The arrows mark some representative optical transitions.

picture [37]. Under a magnetic field, the semiclassical orbit of electronic motion in momentum space resides on the intersection between a constant energy surface and a plane perpendicular to the field direction. By tuning $\boldsymbol{B}$ away from linear tilt direction (z-direction), the semiclassical orbit of type-II C-1 WP changes from a circle to an open trajectory,

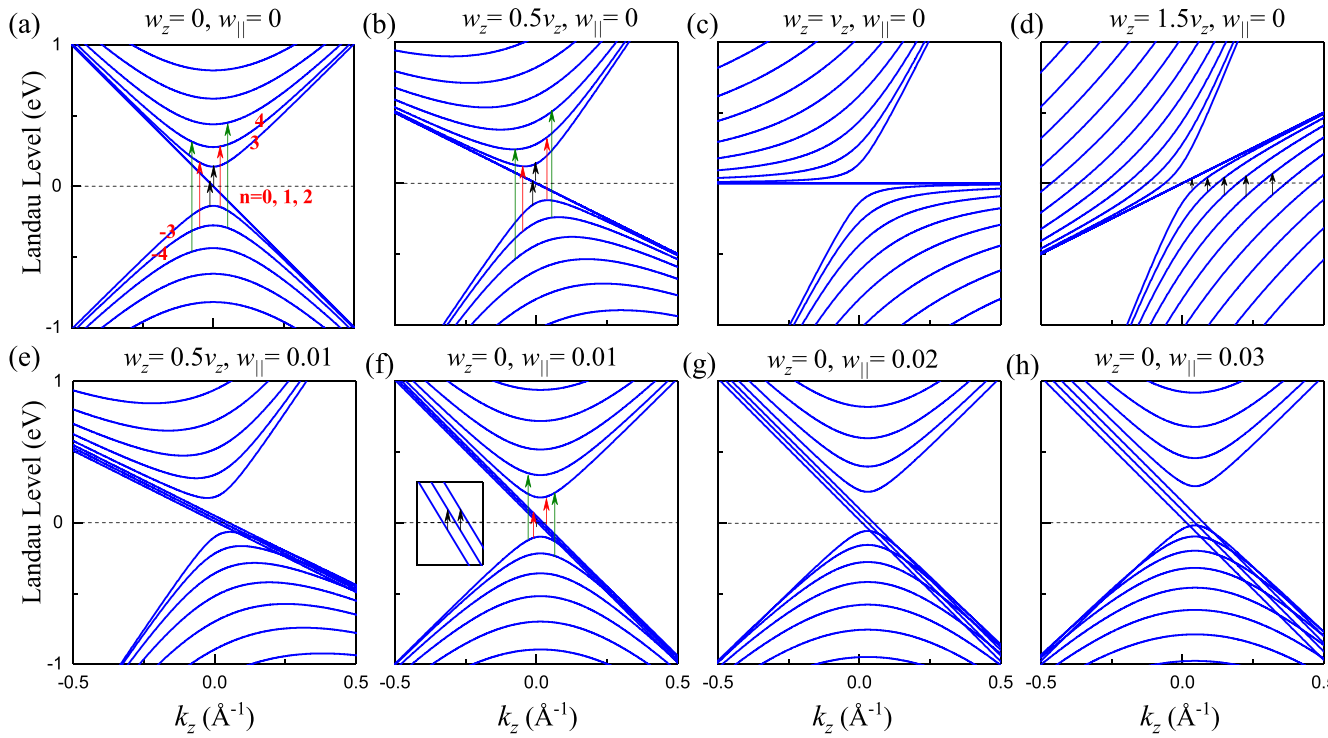

FIG. 2. LL spectrum of the C-3 WPs along k_z with different energy tilts. We set $v_z = 2$ eV Å, $\lambda = 0.02$ eV Å^3, and $l_B = 1$ Å. The arrows mark some representative optical transitions. The units of the parameters of the quadratic tilt $w_{||}$ are eV Å^2.

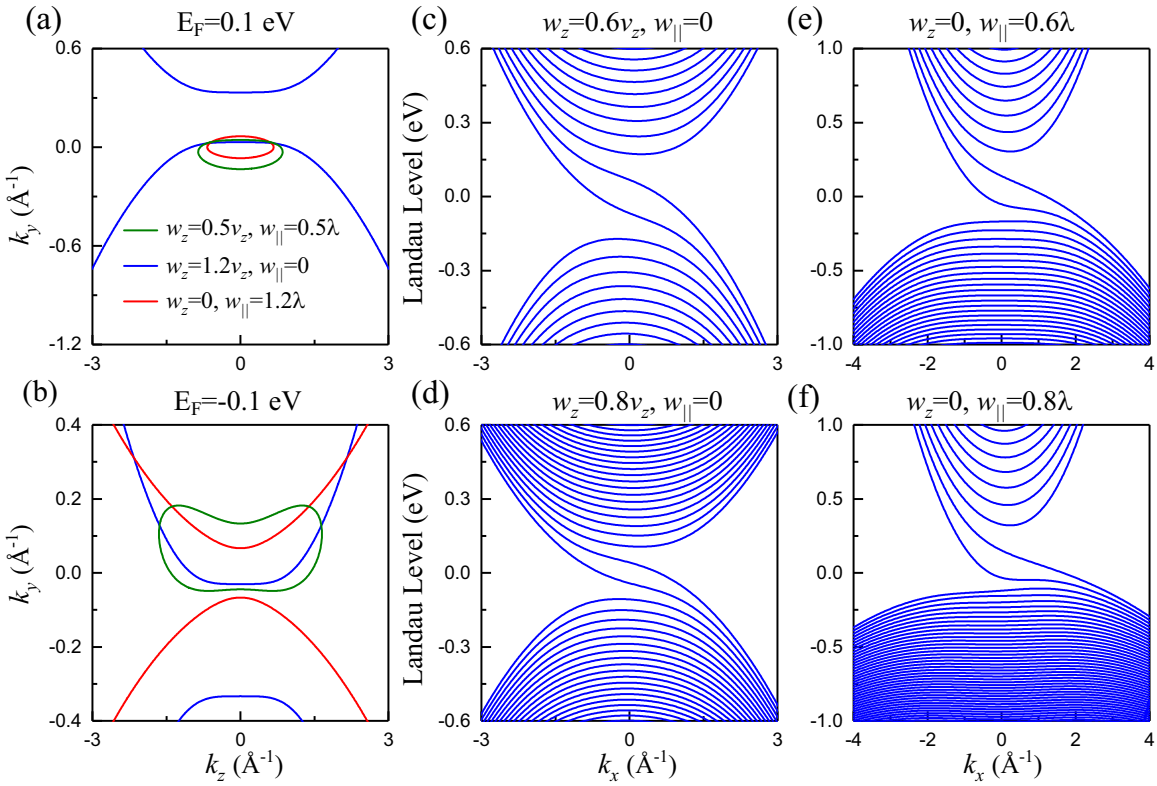

FIG. 3. LL spectrum of C-2 WP for $\boldsymbol{B} \parallel x$. (a),(b) Semiclassical orbit of type I (green solid line), II (blue solid line), and III (red solid line) C-2 WPs at $k_x = 0$ plane for (a) conduction band and (b) valence band. (c)–(f) LL spectrum of C-2 WP with different energy tilts for $l_B = 1$ Å. We set $v_z = 1.5$ eV Å and $\lambda = 0.1$ eV Å^2.

leading to the collapse of LLs [37]. In this work, we show that, when B field deviates from z direction, the type-II C-2 and C-3 WPs also feature the LL collapse for both conduction and valence bands. But, for type-III C-2 WP, only the LL spectrum of the valence (conduction) band collapses when $w_\parallel > 0$ ($w_\parallel < 0$) and the type-III C-3 WP generally does not feature LL collapse.

To explicitly show this, we plot the constant energy surface of the C-2 and C-3 WPs with $k_x = 0$, i.e., we assume B field along x direction, for different linear and quadratic energy tilt in Figs. 3(a), 3(b) and 4(a), 4(b). One can find that, for type-I (type-II) C-2 and C-3 WPs, the constant energy surfaces are always closed (open). In sharp contrast, for type-III C-2 WP, the constant energy surface of the conduction band is still closed but that of the valence band becomes an open trajectory [see the red line in Figs. 3(a) and 3(b)]. And no open constant energy surface can be found in type-III C-3 WP [see the red line in Figs. 4(a) and 4(b)], as the $\pm\lambda k_\parallel^3$ dominates the band structure for large $k_\parallel$.

We also numerically calculate the LLs of C-2 and C-3 WPs for $\boldsymbol{B} \parallel x$ in the region before collapse. The results show that when approaching the phase boundary between type-I and type-II, the LL spacing becomes smaller and smaller, as shown in Figs. 3(c), 3(d) and 4(c), 4(d). When the LL spacing vanishes, the LLs collapse. However, the LL spacing of the valence (conduction) band of C-2 WP becomes smaller and smaller (larger) when increasing the quadratic tilt ($w_{||} > 0$), as shown in Figs. 3(e)and 3(f). Figures 4(e) and 4(f) show that, while the LL spacing of C-3 WP also varies with $w_\parallel$, it generally does not approach zero and hence the LLs will not collapse, consistent with the semiclassical analysis.

B. C-4 WP

Different from the C-2 and C-3 WPs, which can appear at high-symmetry points and lines, the C-4 WP only appear at the high-symmetry points with $\mathcal{T}$ or $\mathcal{T}'$ symmetry [6–8]. Hence the C-4 WP only has quadratic energy tilt, and a general form of the effective Hamiltonian of C-4 is [6]

$$\mathcal{H}_{C-4} = w_{||}k^2 + c_1 k_x k_y k_z \sigma_y + \sqrt{3}c_2\left(k_x^2 - k_y^2\right)\sigma_x + c_2\left(k_x^2 + k_y^2 - 2k_z^2\right)\sigma_z, \tag{20}$$

where $k = \sqrt{k_x^2 + k_y^2 + k_z^2}$, $w_{||}$ denotes the strength of quadratic energy tilt, and $c_{1(2)}$ is real model parameters. The energy dispersion of C-4 WP reads

$$E_\pm = w_{||}k^2 \pm \sqrt{4c_2^2k^4 - 12c_2^2 g(k) + c_1^2 k_x^2 k_y^2 k_z^2}, \tag{21}$$

where $g(k) = k_x^2k_y^2 + k_y^2k_z^2 + k_z^2k_x^2$. Because of the complexity of Eq. (20), it is difficult to solve the LLs and eigenvector of C-4 WPs analytically. Hence, in following calculations, we numerically calculate the LL spectrum of C-4 WP with different quadratic energy tilt. As shown in Fig. 5(a), without any tilt, there are four nondegenerated chiral LLs crossing the zero energy. By adding the quadratic energy tilt, the both chiral and achiral LL bands are elevated, but the elevation is more significant for the chiral LLs in the $k_z > 0$ region. Moreover, we find that, increasing $w_{||} > 0$, the LLs of the

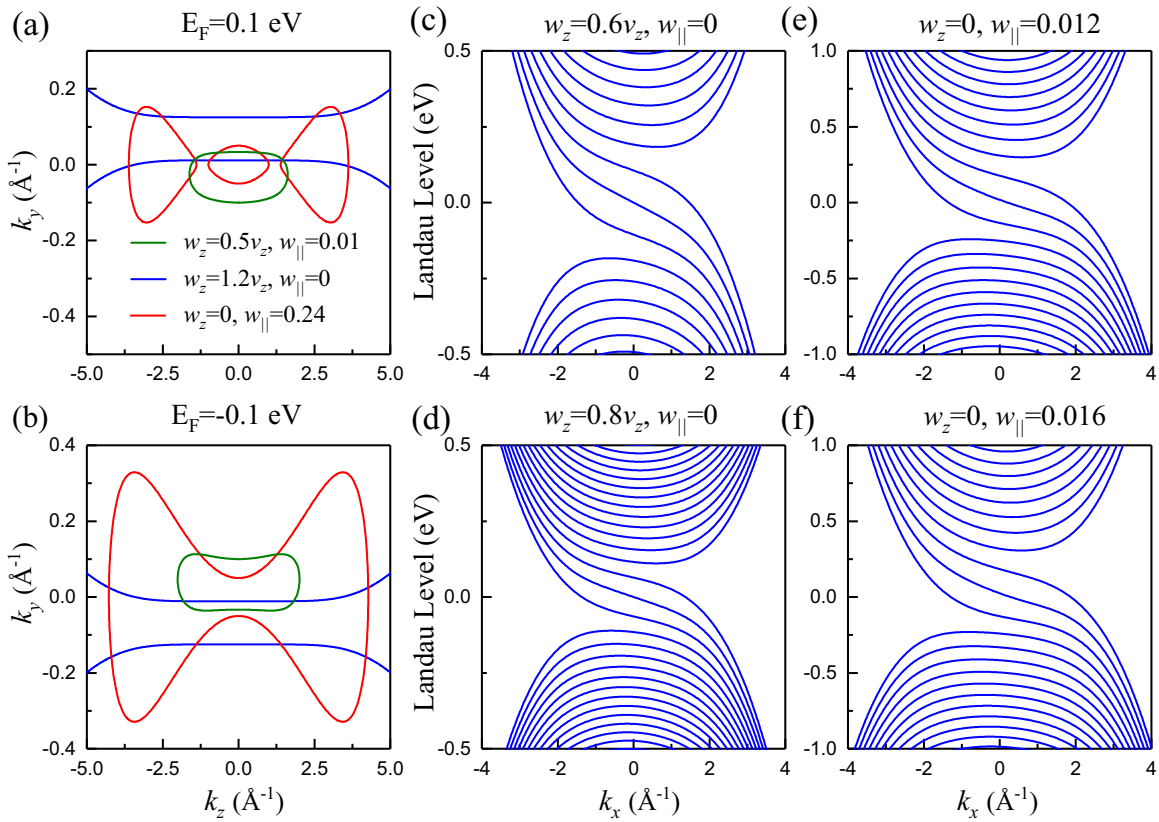

FIG. 4. LL spectrum of C-3 WP for $\boldsymbol{B} \parallel x$. (a),(b) Semiclassical orbit of type I (green solid line), II (blue solid line), and III (red solid line) C-3 WPs at $k_x = 0$ plane for (a) conduction band and (b) valence band. (c)–(f) LL spectrum of C-3 WP with different energy tilts for $l_B = 1$ Å. We set $v_z = 2$ eV Å and $\lambda = 0.02$ eV Å^3. The units of the parameters of the quadratic tilt ($w_{||}$) are eV Å^2.

valence band will be squeezed while that of the conduction band are broadened.

Again, we study the possibility of LL collapse in C-4 WP. From Eq. (21), one knows that the C-4 WP exhibits a leading order of cubic along the (111) direction (as well as the directions symmetry connected to it) and of quadratic along other directions. Hence, when the energy tilt $w_{||}$ is large enough and tuning $\boldsymbol{B}$ away from the z direction, the semiclassical orbit of C-4 WP will go from closed to open, leading to the collapse of LLs. To explicitly show it, we rotate the coordinate axis of the system, causing $k_{x,y,z}$ to be $q_{x,y,z}$. Here, q_z is along the original (111) direction. We plot the constant energy surface of the C-4 WP with $q_y = 0$, i.e., we assume the B field along the (111) direction, for different quadratic energy tilt in Figs. 6(a) and 6(b). One can find that, when $w_{||}$ is large ($w_{||} > 0$), the constant energy surfaces of the conduction (valence) band are always closed (open). We also numerically calculate the LLs of C-4 WPs for B along (111) direction before collapse. The results show that the LL spacing of the valence (conduction) band of C-4 WP becomes smaller and smaller (larger) when increasing the quadratic tilt $w_{||} > 0$, as shown in Figs. 6(c) and 6(d). The spacing of LL for the valence (conduction) band approaches zero and the LL spectrum of the valence (conduction) band collapses when the $w_{||}$ is large enough ($w_{||} > 0$).

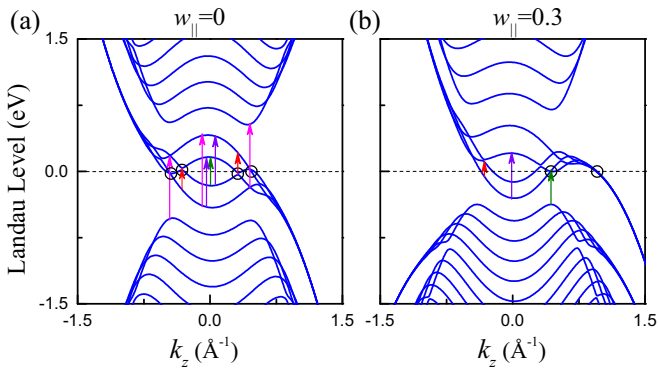

FIG. 5. LL spectrum of the C-4 WP along k_z with different quadratic energy tilt. We set $c_1 = 1$ eV Å^3, $c_2 = 1$ eV Å^2, and $l_B = 3.16$ Å. The unit of $w_{||}$ is eV Å^2.

III. MAGNETO-OPTICAL CONDUCTIVITY

In this section, we study the magneto-optical conductivity of a single unconventional WP with different topological charge and energy tilt. The dynamical conductivity tensor can be obtained from the Kubo formula [49,50]. Here, we focus on the absorptive part of the magneto-optical conductivity with a uniform magnetic field $\boldsymbol{B} \parallel z$. Expressed in the Landau level basis in the clean limit, we have [49,50]

$$\sigma_{ij}(\omega) = \frac{-i\hbar e^2}{2\pi l_B^2} \sum_{n,n'} \int dk_z \frac{\Delta f \langle n, k_z | v_i | n', k_z \rangle \langle n, k_z | v_j | n', k_z \rangle}{(\varepsilon_n - \varepsilon_{n'})(\hbar\omega + \varepsilon_n - \varepsilon_{n'} + i\eta)}, \tag{22}$$

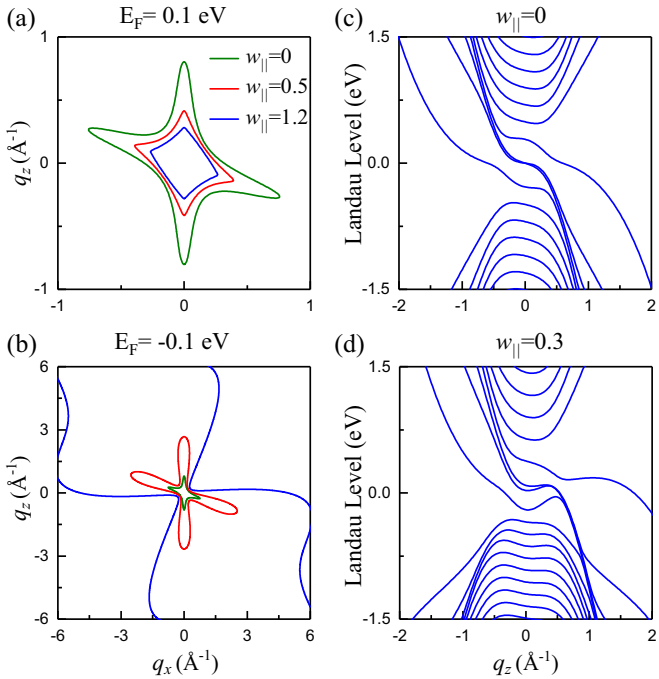

FIG. 6. LL spectrum of C-4 WP for $\boldsymbol{B} \parallel (111)$ direction. Semiclassical orbit of C-4 WPs at $q_y = 0$ plane with different quadratic energy tilts for (a) conduction band and (b) valence band. (c),(d) LL spectrum of C-4 WP with different parameters for $l_B = 3.16$ Å. We set $c_1 = 1$ eV Å^3 and $c_2 = 1$ eV Å^2.

where $i(j) = x, y$, $|n, k_z\rangle$ denotes the LL state, $v_i = \partial_{k_i}\mathcal{H}$ is the velocity operator along the i direction, $\hbar\omega$ is the photon energy, η denotes the scattering rate, $\Delta f = f_n - f_{n'}$ are the occupation differences between the two states involved in the optical transition, and $f(E) = 1/[e^{(E-E_F)/k_BT} + 1]$ is the Fermi-Dirac distribution function with Boltzmann constant k_B and temperature T.

A. Optical transition selection rules

For C-2 and C-3 WPs, the velocity operators v_x and v_y are given by

$$v_x = \omega_1(\hat{a}^\dagger + \hat{a}) + \omega_2[\hat{a}^{m-1}\sigma_+ + (\hat{a}^\dagger)^{m-1}\sigma_-], \quad (23)$$

$$v_y = i\omega_1(\hat{a}^\dagger - \hat{a}) + i\omega_2[\hat{a}^{m-1}\sigma_+ - (\hat{a}^\dagger)^{m-1}\sigma_-], \quad (24)$$

where $\omega_1 = \sqrt{2}w_{||}/l_B$ and $\omega_2 = m\lambda(\sqrt{2}/l_B)^{m-1}$ with $m = 2$ ($m = 3$) for C-2 (C-3) WP. By analyzing the above expression of $v_{x(y)}$ and the eigenstates of C-2 [Eqs. (7) and (9)] and C-3 [Eqs. (14) and (16)] WPs, the optical transition selection rules can be inferred, i.e., the optical transitions only happen between the $\pm n$th and $(\pm n \pm 1)$th LLs for both C-2 and C-3 WPs.

Actually, one can find that the effective Hamiltonians of C-2 and C-3 WPs [see Eq. (1)] are invariant under any small rotation along the z direction, leading to an emergent rotation symmetry, which guarantees the dipolar transitions in C-2 and C-3 WPs [51]. Different from the C-2 and C-3 WPs, the C-4 WP does not have the rotation symmetry along any direction; hence both dipolar and nondipolar transitions can be found in C-4 WP.

B. Numerical results of Re[$\sigma_{xx}(\omega)$]

We then investigate the influence of the linear and quadratic energy tilt on the magneto-optical measurements. The calculated results of the absorptive part of the longitudinal magneto-optical conductivity Re[$\sigma_{xx}(\omega)$] of C-2 and C-3 WPs are plotted in Fig. 7 and Fig. 8 (blue solid curves), where the used parameters are the same as those in Fig. 1 and Fig. 2, respectively. By inspecting the LL spectra in Fig. 1 and Fig. 2, we can observe the following features.

First, without any energy tilt, the conductivity includes a series of asymmetric peaks and the peak spacing is proportional to B ($B^{3/2}$) for C-2 (C-3) WPs [see Figs. 7(a) and 8(a)]. This can be directly obtained by checking the LL spectrum [Eqs. (8) and (15)], where the energy extremal points reside at the $k_z = 0$ point [see Figs. 1(a) and 2(a)]. The positions of the peaks can be easily obtaining by analyzing the transitions happening between the LLs in $k_z = 0$ plane.

Second, Re[$\sigma_{xx}(\omega)$] does not have a dependence on linear energy tilt in the type-I phase [see Figs. 7(a), 7(b) and 8(a), 8(b)], but shows distinctive features in the type-II phase. Since the Weyl cone is overtilted in the type-II phase and the system becomes a metal rather than a semimetal, the Fermi level will cross both chiral and achiral LLs and, in such case, many transitions that can (not) happen in the type-I phase are forbidden (occur), as shown in Figs. 7(d) and 8(d). As a consequence, many absorption peaks appear at low frequencies and the shape of the original peaks are changed from exhibiting long tails to tailless. These are similar to the case in C-1 WP [37].

Third, as aforementioned, the quadratic energy tilt breaks the degeneracy of the two (three) chiral LLs of C-2 (C-3) WP. This leads to two interesting results. One is the transition between chiral LLs, giving rise to one additional peak at low frequencies, as shown in Fig. 7(f) and Fig. 8(f), respectively (marked by the black arrows). Remarkably, we find that the position of these additional peaks is $2w_{||}/l_B^2$, indicating that the peak position can be tuned by the strength of the $\boldsymbol{B}$ field and the quadratic energy tilt. The other interesting result is that the energy degeneracy of the transitions involving chiral LLs also is broken. For C-2 WP with $w_{||} = 0$, the transition energy for $-2 \to 1$ and that for $1 \to 2$ are the same, and for C-3 WP $-3 \to 2$ and $2 \to 3$ are the same, which is marked by red arrow in Fig. 1(a) and Fig. 2(a). In the presence of finite $w_{||}$, these degeneracies are broken and then the original peaks in conductivity are split, as shown in Figs. 7(f) and 8(f) (marked by red arrows). In addition, the quadratic energy tilt also modifies the energy of achiral LLs of both C-2 and C-3 WPs, making the transition energy between $-|n| \to |n| - 1$ and $-(|n| - 1) \to |n|$ no longer the same. Thus the peaks resulting from transitions between the achiral bands also undergo splitting, as indicated by the green arrows in Fig. 1(f) and Fig. 7(f), and those in Fig. 2(f) and Fig. 8(f).

Fourth, for type-III C-2 WP, there also exists the invariable presence of absorption peaks at low frequencies due to the metal feature [see Fig. 7(h)]. But, for type-III C-3 WPs, the LLs of conduction and valence bands generally are separated in energy, when the strength of the B field is large or $w_{\parallel}$ is

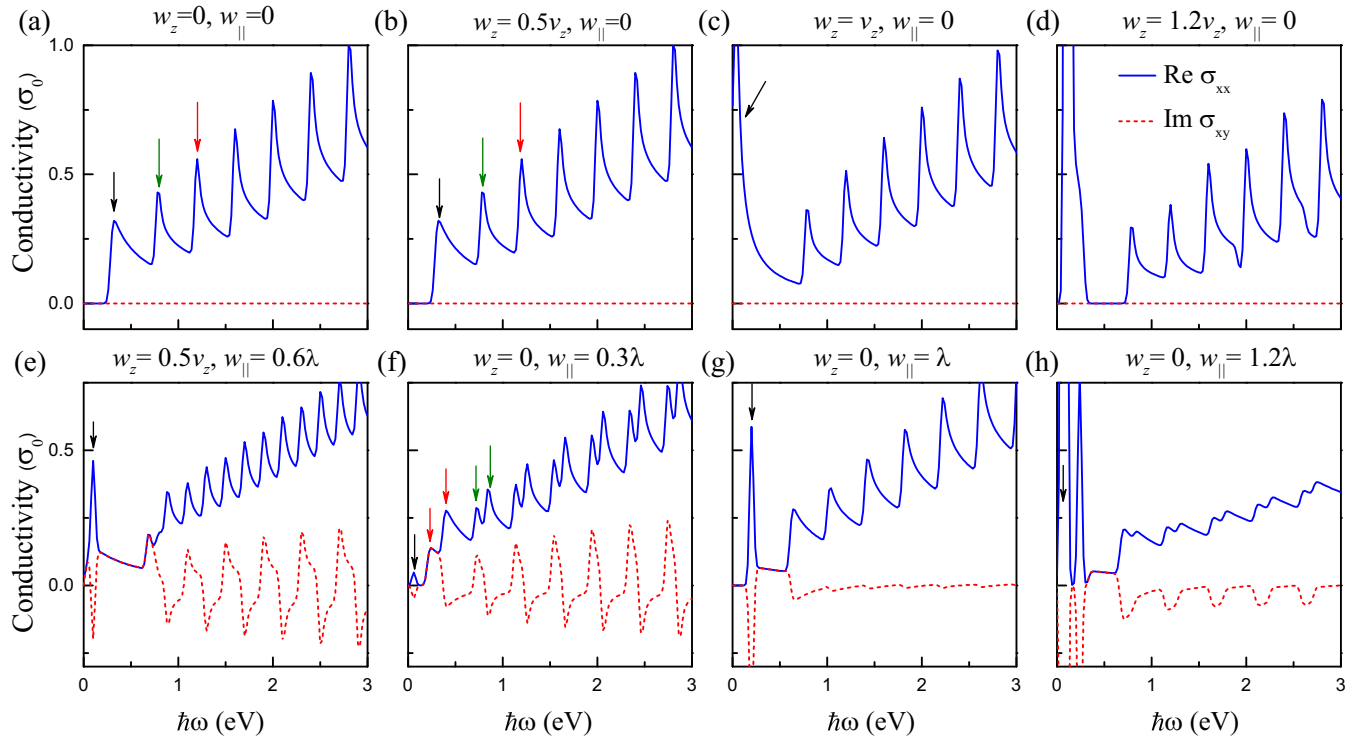

FIG. 7. Re[$\sigma_{xx}(\omega)$] (blue solid curves) and Im[$\sigma_{xy}(\omega)$] (red dashed curves) plotted for the C-2 WPs with linear and quadratic tilt terms, in units of $\sigma_0 = \frac{\hbar e^2}{2\pi l_B^2}$, and the used parameters are the same as those in Fig. 1. The black, red, and green arrows correspond to the transitions between the different subbands in Fig. 1. We set $\eta = 2 \times 10^{-2}$ eV.

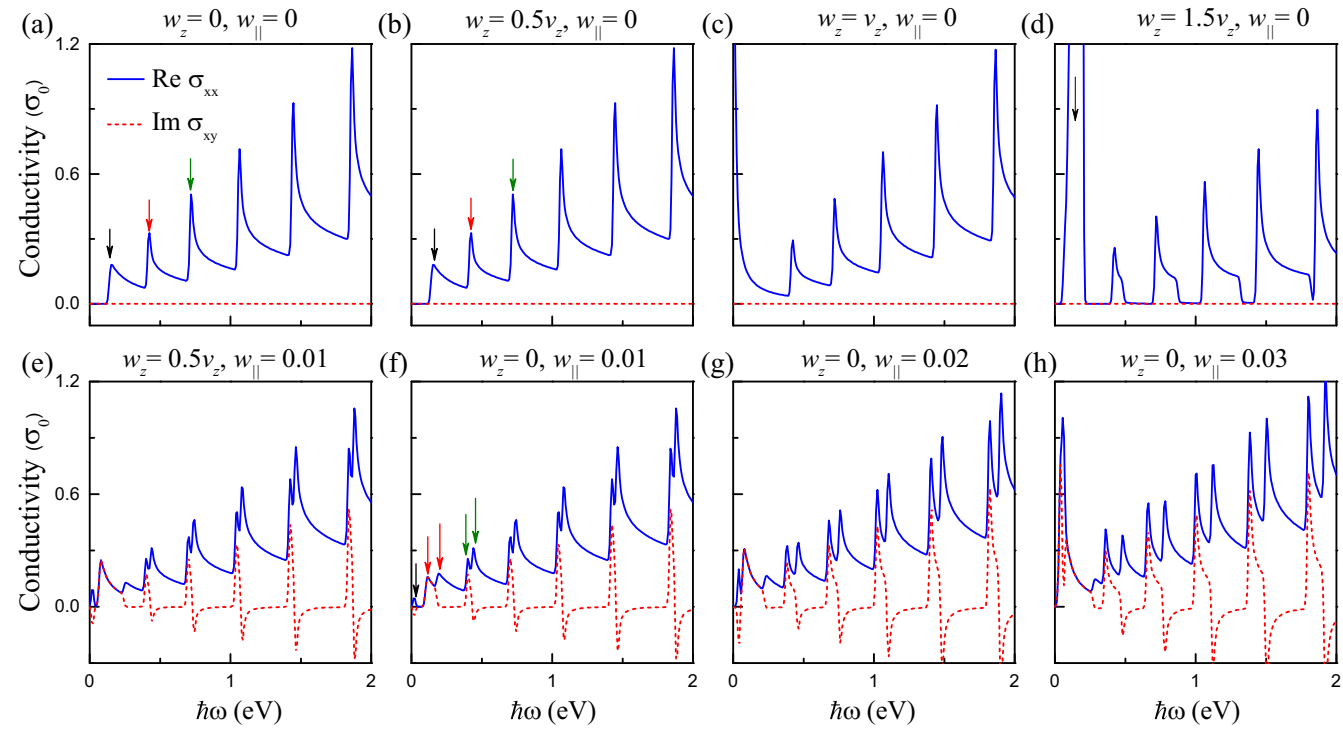

FIG. 8. Re[$\sigma_{xx}(\omega)$] (blue solid curves) and Im[$\sigma_{xy}(\omega)$] (red dashed curves) plotted for the C-3 WPs with linear and quadratic tilt terms, in units of $\sigma_0 = \frac{\hbar e^2}{2\pi l_B^2}$ and the used parameters are the same as those in Fig. 2. The black, red, and green arrows correspond to the transitions between the different subbands in Fig. 2. We set $\eta = 8 \times 10^{-3}$ eV.

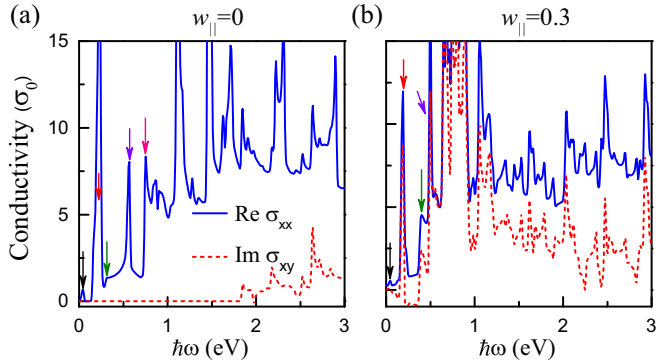

FIG. 9. Re$[\sigma_{xx}(\omega)]$ (blue solid curves) and Im$[\sigma_{xy}(\omega)]$ (red dashed curves) plotted for the C-4 WPs with quadratic tilt terms, in units of $\sigma_0 = \frac{\hbar e^2}{2\pi l_B^2}$, and the used parameters are the same as those in Fig. 5. The red and green arrows correspond to the transitions between the different subbands in Fig. 5. The black arrows correspond to the transitions that occur at the k point marked by the black circle in Fig. 5. We set $\eta = 8 \times 10^{-3}$ eV.

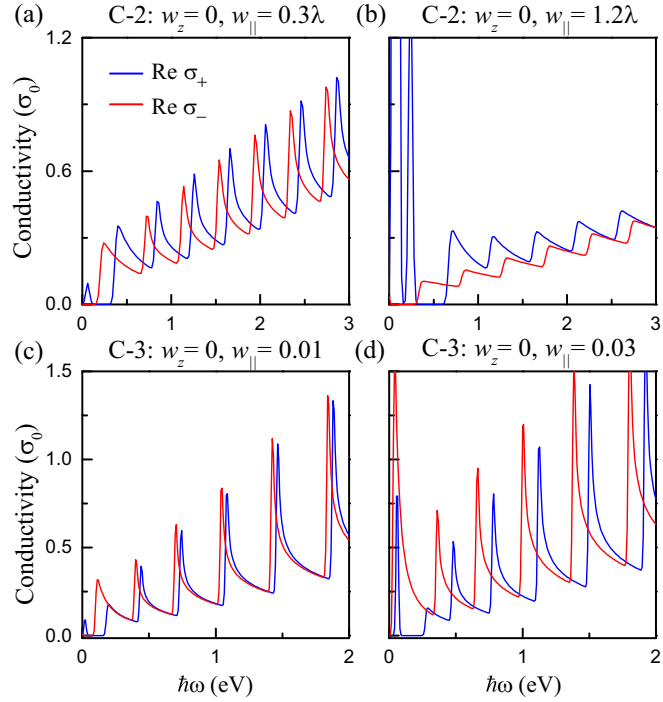

FIG. 10. Re$[\sigma_+(\omega)]$ (blue solid curves) and Re$[\sigma_-(\omega)]$ (red solid curves) plotted for the (a),(b) C-2 and (c),(d) C-3 WPs in units of $\sigma_0 = \frac{\hbar e^2}{2\pi l_B^2}$. (a),(b) and (c),(d) correspond to Figs. 7(f), 7(h) and Figs. 8(f), 8(h), respectively.

small. Hence the type-III C-3 WP may or may not exhibit significant absorption peaks at low frequencies, depending on the model parameters, as shown in Figs. 8(f)–8(h).

At last, we discuss the magneto-optical conductivity of C-4 WP, the results of which are plotted in Fig. 9. One observes that the magneto-optical conductivity of C-4 WP is irregular due to the complexity of the corresponding LLs, completely differing from that of C-2 and C-3 WPs. Thus the influence of quadratic energy tilt on the magneto-optical conductivity also is subtle and may have a strong dependence on the model parameters and the strength of the B field. But two key observations can be inferred from the LLs and Fig. 9. Since the four chiral LLs in C-4 WP are always not degenerate, the C-4 WP inevitably exhibits several transition peaks at low energy, as labeled by the arrows in Fig. 9. Besides, there is almost an absorption peak around the zero-energy position, as the Fermi level always crosses the intersection of two subbands, as marked by the black circles in Fig. 5.

C. Numerical results of Im$[\sigma_{xy}(\omega)]$ and Re$[\sigma_{\pm}(\omega)]$

In this subsection, we study the transverse magneto-optical conductivity $\sigma_{xy}(\omega)$, as well as the conductivity under circularly polarized light $\sigma_{\pm}(\omega) = \sigma_{xx}(\omega) \pm i\sigma_{xy}(\omega)$. The absorptive part of these two conductivities are Im$[\sigma_{xy}(\omega)]$ and Re$[\sigma_{\pm}(\omega)]$. Notice that the circularly polarized light $\sigma_{\pm}$ exhibits certain orbital angular momentum of ± 1. Hence, under left (right) circularly polarized light σ_- (σ_+), only the transitions between the $\pm n$th and $(\pm n - 1)$th [$\pm n$th and $(\pm n + 1)$th] LLs happen for C-2 and C-3 WPs.

The calculated results of Im$[\sigma_{xy}(\omega)]$ of C-2 and C-3 WPs also are plotted in Fig. 7 and Fig. 8 (red dashed curves). Interestingly, Im$[\sigma_{xy}(\omega)]$ vanishes for the C-2 and C-3 WPs without quadratic energy tilt, as shown in Figs. 7(a)–7(d) and Figs. 8(a)–8(d). As discussed above, the possible optical transition for C-2 and C-3 WPs under linearly polarized light are from $-|n| \to |n| \pm 1$ LLs. In the absence of the quadratic energy tilt $w_{||} = 0$, the two processes $-|n| \to |n| - 1$ and $-(|n| - 1) \to |n|$ exhibit the same frequency but opposite contribution to Im$[\sigma_{xy}(\omega)]$, leading to vanishing Im$[\sigma_{xy}(\omega)]$ for all the frequency. But when the quadratic energy tilt $w_{||}$ is finite, the frequencies of the two processes $-|n| \to |n| - 1$ and $-(|n| - 1) \to |n|$ are no longer the same. Hence the Im$[\sigma_{xy}(\omega)]$ show a series of positive and negative peaks when $w_{||}$ is not very large, as shown in Figs. 7(e)–7(g) and Figs. 8(e)–8(h). For type-III C-2 WP, almost all the peaks of Im$[\sigma_{xy}(\omega)]$ are negative [see Fig. 7(h)].

Moreover, one can find that the Re$[\sigma_{xx}(\omega)]$ equals Im$[\sigma_{xy}(\omega)]$ at certain frequencies [see Figs. 7(d)–7(h) and Figs. 8(d)–8(h)] as, in these frequency ranges, only the transitions $-|n| \to |n| - 1$ exist. This can be more clearly understood in the results of Re$[\sigma_{\pm}(\omega)]$, which are shown in Fig. 10. In these frequency ranges, Re$[\sigma_+(\omega)] =$ Re$[\sigma_{xx}(\omega)] -$ Im$[\sigma_{xy}(\omega)]$ is zero, which is consistent with the physics that Re$[\sigma_+(\omega)]$ is solely induced by the transitions between the $\pm n$th and $(\pm n + 1)$th LLs and then must vanish in the frequency ranges that do not have this kind of transition. Also, the number of peaks in Re$[\sigma_{\pm}(\omega)]$ is about half that in Re$[\sigma_{xx}(\omega)]$ and Im$[\sigma_{xy}(\omega)]$, as a linearly polarized light can be considered as a combination of left and right circularly polarized light.

Again, we find that Im$[\sigma_{xy}(\omega)]$ and Re$[\sigma_{\pm}(\omega)]$ of C-4 WP are irregular, which can be inferred from Fig. 9, as all the transitions including dipolar and nondipolar transitions can be realized in C-4 WP for both linearly and circularly polarized light.

IV. SUMMARY

In summary, based on the low-energy effective Hamiltonian and Kubo formula, we have systematically studied the magnetoresponse of WPs with both linear and quadratic energy tilt and with a topological charge of $n = 2, 3, 4$. We find that the magnetoresponses of these systems with linear and that with quadratic energy tilt exhibit completely different signatures. For C-2 and C-3 WPs, the linear energy tilt always tends to squeeze the LLs of both conduction and valence bands, and eventually leads to LL collapse in the type-II phase. In contrast, for C-2 and C-4 WPs, the quadratic energy tilt tends to squeeze the LLs of either the valence or the conduction band and broadens the LLs of the other one. Hence, when quadratic energy tilt is large and the C-2 (C-4) WP becomes the type-III one, only valence or conduction band features LLs collapse. Interestingly, the LL collapse generally cannot be realized in C-3 WP regardless of the presence or absence of the quadratic energy tilt.

For $\mathrm{Re}[\sigma_{xx}(\omega)]$, we also find that, for type-I WPs, it does not have a dependence on the linear energy tilt. But when the linear energy tilt is large enough and the type-I WPs become type-II ones, many additional absorption peaks appear at low frequencies. In contrast, the degeneracy of the chiral LLs for C-2 and C-3 WPs can be broken by the quadratic energy tilt, which makes a new transition between the chiral LLs and leads to one additional peak in the longitudinal conductivity spectrum at low frequencies. The modification of LL bands caused by quadratic tilt also leads to the splitting of the original longitudinal conductivity peaks induced by the transitions between achiral LLs. The transition between different chiral LLs always can be found in C-4 WP, as the four chiral LLs in C-4 WP are not degenerate whether or not there is a quadratic energy tilt.

We also investigate the behavior of $\mathrm{Im}[\sigma_{xy}(\omega)]$ and the magneto-optical conductivity of the unconventional WPs under circularly polarized light $\mathrm{Re}[\sigma_{\pm}(\omega)]$. We find that $\mathrm{Im}[\sigma_{xy}(\omega)]$ vanishes for C-2 and C-3 Weyl points without quadratic energy tilt and exhibits a series of positive and negative peaks when the quadratic energy tilt is not very large. The behavior of $\mathrm{Re}[\sigma_{\pm}(\omega)]$ then can be easily obtained from the longitudinal and transverse magneto-optical conductivities and our results are consistent with the physics analysis.

Note added. Recently, we became aware of Ref. [52], which studied the magneto-optical conductivity of the type-I and type-II C-n ($n = 1, 2, 3$) WPs with closed Fermi surface.

ACKNOWLEDGMENTS

The authors thank J. Xun for helpful discussions. This work was supported by the NSF of China (Grants No. 12004035, No. 12234003, and No. 12061131002), the National Key R&D Program of China (Grant No. 2020YFA0308800), the National Natural Science Fund for Excellent Young Scientists Fund Program (Overseas), and Beijing Institute of Technology Research Fund Program for Young Scholars.

[1] N. P. Armitage, E. J. Mele, and A. Vishwanath, Weyl and dirac semimetals in three-dimensional solids, Rev. Mod. Phys. **90**, 015001 (2018).

[2] P. Hosur and X. Qi, Recent developments in transport phenomena in Weyl semimetals, C. R. Phys. **14**, 857 (2013).

[3] X. Wan, A. M. Turner, A. Vishwanath, and S. Y. Savrasov, Topological semimetal and Fermi-arc surface states in the electronic structure of pyrochlore iridates, Phys. Rev. B **83**, 205101 (2011).

[4] G. Xu, H. Weng, Z. Wang, X. Dai, and Z. Fang, Chern Semimetal and the Quantized Anomalous Hall Effect in $HgCr_2Se_4$, Phys. Rev. Lett. **107**, 186806 (2011).

[5] C. Fang, M. J. Gilbert, X. Dai, and B. A. Bernevig, Multi-Weyl Topological Semimetals Stabilized by Point Group Symmetry, Phys. Rev. Lett. **108**, 266802 (2012).

[6] Z.-M. Yu, Z. Zhang, G.-B. Liu, W. Wu, X.-P. Li, R.-W. Zhang, S. A. Yang, and Y. Yao, Encyclopedia of emergent particles in three-dimensional crystals, Sci. Bull. **67**, 375 (2022).

[7] G.-B. Liu, Z. Zhang, Z.-M. Yu, S. A. Yang, and Y. Yao, Systematic investigation of emergent particles in type-III magnetic space groups, Phys. Rev. B **105**, 085117 (2022).

[8] Z. Zhang, G.-B. Liu, Z.-M. Yu, S. A. Yang, and Y. Yao, Encyclopedia of emergent particles in type-IV magnetic space groups, Phys. Rev. B **105**, 104426 (2022).

[9] T. Zhang, R. Takahashi, C. Fang, and S. Murakami, Twofold quadruple Weyl nodes in chiral cubic crystals, Phys. Rev. B **102**, 125148 (2020).

[10] Q.-B. Liu, Y. Qian, H.-H. Fu, and Z. Wang, Symmetry-enforced Weyl phonons, npj Comput. Mater. **6**, 95 (2020).

[11] A. A. Soluyanov, D. Gresch, Z. Wang, Q. Wu, M. Troyer, X. Dai, and B. A. Bernevig, Type-II Weyl semimetals, Nature (London) **527**, 495 (2015).

[12] X. P. Li, K. Deng, B. Fu, Y. K. Li, D. S. Ma, J. F. Han, J. Zhou, S. Zhou, and Y. Yao, Type-III Weyl semimetals: $(TaSe_4)_2I$, Phys. Rev. B **103**, L081402 (2021).

[13] T. E. O'Brien, M. Diez, and C. W. J. Beenakker, Magnetic Breakdown and Klein Tunneling in a Type-II Weyl Semimetal, Phys. Rev. Lett. **116**, 236401 (2016).

[14] K. Deng, G. Wan, P. Deng, K. Zhang, S. Ding, E. Wang, M. Yan, H. Huang, H. Zhang, Z. Xu, J. Denlinger, A. Fedorov, H. Yang, W. Duan, H. Yao, Y. Wu, S. Fan, H. Zhang, X. Chen, and S. Zhou, Experimental observation of topological Fermi arcs in type-II Weyl semimetal $MoTe_2$, Nat. Phys. **12**, 1105 (2016).

[15] M.-Y. Yao, N. Xu, Q. S. Wu, G. Autès, N. Kumar, V. N. Strocov, N. C. Plumb, M. Radovic, O. V. Yazyev, C. Felser, J. Mesot, and M. Shi, Observation of Weyl Nodes in Robust Type-II Weyl Semimetal WP_2, Phys. Rev. Lett. **122**, 176402 (2019).

[16] K. Halterman and M. Alidoust, Waveguide modes in Weyl semimetals with tilted dirac cones, Opt. Express **27**, 36164 (2019).

[17] K. Halterman, M. Alidoust, and A. Zyuzin, Epsilon-near-zero response and tunable perfect absorption in Weyl semimetals, Phys. Rev. B **98**, 085109 (2018).

[18] F. Xiong, C. Honerkamp, D. M. Kennes, and T. Nag, Understanding the three-dimensional quantum Hall effect in generic multi-Weyl semimetals, Phys. Rev. B **106**, 045424 (2022).

[19] G. Ding, J. Wang, Z.-M. Yu, Z. Zhang, W. Wang, and X. Wang, Single pair of type-III Weyl points half-metals: $BaNiIO_6$ as an example, Phys. Rev. Mater. **7**, 014202 (2023).

[20] L. Jin, X. Zhang, Y. Liu, X. Dai, L. Wang, and G. Liu, Fully spin-polarized double-Weyl fermions with type-III dispersion in the quasi-one-dimensional materials X_2RhF_6 (X = K, Rb, Cs), Phys. Rev. B **102**, 195104 (2020).

[21] X. Wang, F. Zhou, Z. Zhang, W. Wu, Z.-M. Yu, and S. A. Yang, Single pair of multi-Weyl points in nonmagnetic crystals, Phys. Rev. B **106**, 195129 (2022).

[22] S.-M. Huang, S.-Y. Xu, I. Belopolski, C.-C. Lee, G. Chang, T.-R. Chang, B. Wang, N. Alidoust, G. Bian, M. Neupane, D. Sanchez, H. Zheng, H.-T. Jeng, A. Bansil, T. Neupert, H. Lin, and M. Z. Hasan, Photonic crystals possessing multiple Weyl points and the experimental observation of robust surface states, Proc. Natl. Acad. Sci. USA **113**, 1180 (2016).

[23] Y. Jiang, Z. Dun, S. Moon, H. Zhou, M. Koshino, D. Smirnov, and Z. Jiang, Landau Quantization in Coupled Weyl Points: A Case Study of Semimetal NbP, Nano Lett. **18**, 7726 (2018).

[24] Y. Hayashi, Y. Okamura, N. Kanazawa, T. Yu, T. Koretsune, R. Arita, A. Tsukazaki, M. Ichikawa, M. Kawasaki, Y. Tokura, and Y. Takahashi, Magneto-optical spectroscopy on Weyl nodes for anomalous and topological Hall effects in chiral MnGe, Nat. Commun. **12**, 5974 (2021).

[25] A. Akrap, M. Hakl, S. Tchoumakov, I. Crassee, J. Kuba, M. O. Goerbig, C. C. Homes, O. Caha, J. Novák, F. Teppe, W. Desrat, S. Koohpayeh, L. Wu, N. P. Armitage, A. Nateprov, E. Arushanov, Q. D. Gibson, R. J. Cava, D. van der Marel, B. A. Piot, C. Faugeras, G. Martinez, M. Potemski, and M. Orlita, Magneto-Optical Signature of Massless Kane Electrons in Cd_3As_2, Phys. Rev. Lett. **117**, 136401 (2016).

[26] B. Xu, Y. M. Dai, L. X. Zhao, K. Wang, R. Yang, W. Zhang, J. Y. Liu, H. Xiao, G. F. Chen, A. J. Taylor, D. A. Yarotski, R. P. Prasankumar, and X. G. Qiu, Optical spectroscopy of the Weyl semimetal TaAs, Phys. Rev. B **93**, 121110(R) (2016).

[27] P. E. C. Ashby and J. P. Carbotte, Chiral anomaly and optical absorption in Weyl semimetals, Phys. Rev. B **89**, 245121 (2014).

[28] S. Ahn, E. J. Mele, and H. Min, Optical conductivity of multi-Weyl semimetals, Phys. Rev. B **95**, 161112(R) (2017).

[29] D. Neubauer, J. P. Carbotte, A. A. Nateprov, A. Löhle, M. Dressel, and A. V. Pronin, Interband optical conductivity of the [001]-oriented Dirac semimetal Cd_3As_2, Phys. Rev. B **93**, 121202(R) (2016).

[30] C. J. Tabert, J. P. Carbotte, and E. J. Nicol, Optical and transport properties in three-dimensional Dirac and Weyl semimetals, Phys. Rev. B **93**, 085426 (2016).

[31] C. J. Tabert and J. P. Carbotte, Optical conductivity of Weyl semimetals and signatures of the gapped semimetal phase transition, Phys. Rev. B **93**, 085442 (2016).

[32] M. Alidoust and K. Halterman, Controllable nonreciprocal optical response and handedness-switching in magnetized spin-orbit coupled graphene, Phys. Rev. B **105**, 045409 (2022).

[33] P. E. C. Ashby and J. P. Carbotte, Magneto-optical conductivity of Weyl semimetals, Phys. Rev. B **87**, 245131 (2013).

[34] J. D. Malcolm and E. J. Nicol, Analytic evaluation of Kane fermion magneto-optics in two and three dimension, Phys. Rev. B **94**, 224305 (2016).

[35] J. M. Shao and G. W. Yang, Magneto-optical conductivity of Weyl semimetals with quadratic term in momentum, AIP Adv. **6**, 025312 (2016).

[36] Y. Sun and A.-M. Wang, Magneto-optical conductivity of double Weyl semimetals, Phys. Rev. B **96**, 085147 (2017).

[37] Z.-M. Yu, Y. Yao, and S. A. Yang, Predicted Unusual Magnetoresponse in Type-II Weyl Semimetals, Phys. Rev. Lett. **117**, 077202 (2016).

[38] M. Udagawa and E. J. Bergholtz, Field-Selective Anomaly and Chiral Mode Reversal in Type-II Weyl Materials, Phys. Rev. Lett. **117**, 086401 (2016).

[39] S. Tchoumakov, M. Civelli, and M. O. Goerbig, Magnetic-Field-Induced Relativistic Properties in Type-I and Type-II Weyl Semimetals, Phys. Rev. Lett. **117**, 086402 (2016).

[40] M. Stålhammar, J. Larana-Aragon, J. Knolle, and E. J. Bergholtz, Magneto-optical conductivity in generic Weyl semimetals, Phys. Rev. B **102**, 235134 (2020).

[41] Y. J. Jin, Y. Xu, Z. J. Chen, and H. Xu, Type-II quadratic and cubic Weyl fermions, Phys. Rev. B **105**, 035141 (2022).

[42] S. F. Shivam Yadav and I. Mandal, Magneto-transport signatures in periodically-driven Weyl and multi-Weyl semimetals, Phys. E **144**, 115444 (2022).

[43] Y. Gao and F. Zhang, Current-induced second harmonic generation of Dirac or Weyl semimetals in a strong magnetic field, Phys. Rev. B **103**, L041301 (2021).

[44] C. Cui, X.-P. Li, D.-S. Ma, Z.-M. Yu, and Y. Yao, Charge-four Weyl point: Minimum lattice model and chirality-dependent properties, Phys. Rev. B **104**, 075115 (2021).

[45] G. Sundaram and Q. Niu, Wave-packet dynamics in slowly perturbed crystals: Gradient corrections and Berry-phase effects, Phys. Rev. B **59**, 14915 (1999).

[46] D. Xiao, M.-C. Chang, and Q. Niu, Berry phase effects on electronic properties, Rev. Mod. Phys. **82**, 1959 (2010).

[47] T. Cai, S. A. Yang, X. Li, F. Zhang, J. Shi, W. Yao, and Q. Niu, Magnetic control of the valley degree of freedom of massive Dirac fermions with application to transition metal dichalcogenides, Phys. Rev. B **88**, 115140 (2013).

[48] J.-W. Rhim, K. Kim, and B.-J. Yang, Quantum distance and anomalous Landau levels of flat bands, Nature (London) **584**, 59 (2020).

[49] T. Ando and Y. Uemura, Theory of Quantum Transport in a Two-Dimensional Electron System under Magnetic Fields. I. Characteristics of Level Broadening and Transport under Strong Fields, J. Phys. Soc. Jpn. **36**, 959 (1974).

[50] G. D. Mahan, *Many-Particle Physics*, 3rd ed. (Springer, Berlin, 2000).

[51] J. Sári, M. O. Goerbig, and C. Tőke, Magneto-optics of quasirelativistic electrons in graphene with an inplane electric field and in tilted Dirac cones in α-(BEDT TTF)$_2$I$_3$, Phys. Rev. B **92**, 035306 (2015).

[52] S. Yadav, S. Sekh, and I. Mandal, Magneto-optical conductivity in the type-I and type-II phases of Weyl/multi-Weyl semimetals, arXiv:2207.03316.